Proceedings of the ASME 2012 Fluids Engineering Summer Meeting
FEDSM2012
July 8-12, 2012, Rio Grande, Puerto Rico

FEDSM2012-72108

Flow Visualization using Cavitation within Blade Passage of an Axial Waterjet Pump Rotor

David Y. Tan
Dept. of Mechanical Engineering
Johns Hopkins University
Baltimore, MD, USA

Rinaldo L. Miorini
Dept. of Mechanical Engineering
Johns Hopkins University
Baltimore, MD, USA

Jens Keller
Dept. of Energy
Universidad de Oviedo
Gijon, Spain

Joseph Katz
Dept. of Mechanical Engineering
Johns Hopkins University
Baltimore, MD, USA

ABSTRACT

Cavitation phenomena within an axial waterjet pump, AxWJ-2 [1,2] operating at and below the best efficiency point (BEP) are investigated using high-speed imaging. The purpose of these preliminary observations is to provide an overview of the physical appearance of several forms of cavitation under varying flow and pressure conditions. These observations provide a motivation for upcoming detailed velocity and turbulence measurements. The experiment is conducted using a transparent pump installed in an optically index-matched facility, which facilitates unobstructed visual access to the pressure and suction sides of the rotor and stator blade passages. By varying the cavitation index within the facility, the observations follow the gradual development of cavitation from inception level to conditions under which the cavitation covers the entire blade. Cavitation appears first in the tip gap, as the fluid is forced from the pressure side (PS) to the suction side (SS) of the rotor blade. Bubbly streaks start at the SS corner, and penetrate into the passage, and are subsequently entrained into the tip leakage vortex (TLV) propagating in the passage. Sheet cavitation also develops along the SS of the rotor leading edge and covers increasing fractions of the blade surface with decreasing cavitation number. At BEP conditions, the sheet is thin. Below BEP, the blade loading increases as a result of an increase in the incidence angle of the flow entering the passage relative to the blade. Consequently, the backward leakage flow also increases, further increasing the incidence angle in the tip region, and thickening the sheet cavitation there. Consistent with previous observations on swept hydrofoils, a re-entrant jet that flows radially outward develops at the trailing edge of the sheet cavitation. Only near the tip corner the trailing edge of the sheet cavitation is opened as the radial re-entrant flow is entrained into the TLV, forming an unstable and noisy spiraling pattern. Within a certain range of cavitation indices, when the sheet cavitation length at the blade tip extends to about 50-60% of the blade spacing, the sheet cavitation on every other blade begins to expand and contract rapidly, generating loud low-frequency noise. With further decrease in pressure, persistent alternating cavitation occurs, namely, the cavitating region on one blade becomes much larger than that in the neighboring one. The mechanisms involved and associated instabilities are discussed based on previous analyses performed for inducers. As the cavitation number is lowered even further, the sheet cavitation on the "heavily-cavitating" blade grows, and eventually passes the trailing edge of the rotor blade. At this condition, cavitation begins again to expand and contract rapidly on the "less-cavitating" blade, covering a significant portion of SS surface. At a lower pressure, all the blades cavitate, with the sheet cavitation covering the entire SS surface of the rotor blade. The large cavities on alternate rotor blade surfaces re-direct flow into the neighboring passages with the smaller cavities. As a result, there is a lower flow rate in the passage with the larger cavitation and higher flow rate in the neighboring passage. As the flow with the cavitating passage arrives to the leading edge of the stator flow rate, it increases the incidence angle at the entrance to the stator, causing intermittent sheet and cloud cavitation on the stator blade.

INTRODUCTION

It is an understatement to say that the effects of cavitation are a concern for tubomachinery, ship propeller blades, and other hydraulic equipment. There is no shortage of graphic evidence for the damage caused by cavitation [3-5], nor interest in studying cavitation phenomena near boundaries [6-8]. Despite extensive research on the behavior of cavitation in turbomachinery there are still many unanswered questions, especially those associated with instabilities, and is the object of much ongoing research, in great part since the associated

flows and geometries are complex. One of these cavitation phenomena is alternate blade cavitation, which will be discussed in this paper. Alternate blade cavitation has been reported as early as 1958 by Acosta [9]. Since then, efforts have been made to elucidate the physics behind this phenomenon, either in the form of experiments (Bordelon et al. [10], Goirand et al. [11], Huang et al. [12]) or numerical models (Poufarry et al. [13], Semenov and Tsujimoto [14], Horiguchi et al. [15]).

Tsujimoto [16] explains that alternate blade cavitation is a result of a region of altered flow near the trailing edge of a large cavity on a blade surface, where the flow is inclined towards the suction surface of the blade with the large cavity. As a result the incidence angle to the neighboring blade is smaller and hence the cavity length on the neighboring blade will also be smaller. More recently, Poufarry et al. [13] have used numerical simulations to indicate the different regimes of cavitation instability on a cascade, including alternate blade cavitation. Their explanation for this phenomenon has to do with the increase in angle of attack on the blade with the large cavity, and, as a result, there is an increase in pressure on the pressure side of this blade, and an overall increase in pressure in the neighboring passage. Consequently, the attached cavitation on the next blade is smaller.

Another cavitation phenomenon that this paper will highlight is cavitation associated with tip leakage flows. Prior to the current investigation, we conducted a series of experiments on a different axial pump (AxWJ-1) to study tip leakage flows [17-19]. Tip leakage flows cause several adverse effects in turbomachines, such as diminishing overall performance, reduction in efficiency [20-23], as well as causing the onset of stall [24,25] and rotating instabilities [26]. Tip leakage flows are a result of the pressure difference between the pressure and suction sides of a rotor blade, which forces the fluid through the gap between the tip of the blade and the casing endwall. Consequently, the associated circulation rolls up to form a TLV that influences the flow field in the tip region of the rotor blade passage [27]. One of the main challenges in studying the flow within turbomachines is the blade and casing optical obstruction. In order to perform particle image velocimetry (PIV) without these constraints, Uzol et al. [28] have developed a facility, within which the refractive index of the fluid is matched with that of the transparent blades. The cavitation images shown in this paper have been recorded in an upgraded version of this facility, enabling us to identify significant flow phenomena. In the same facility, but using a different waterjet pump, cavitation was used to visualize and follow the development of flow structures associated with the TLV, both at BEP [19] and below-BEP conditions [29]. They showed images of attached cavitation in the tip gap, within the TLV itself as it forms near the SS of one blade, TLV migration from the SS of the originating blade towards the PS of the neighboring blade, and eventually, TLV bursting as it migrates to the vicinity of the neighboring blade. Combining cavitation images with stereocopic particle image velocimetry (SPIV) data, they identify vortex filaments that wrap around the main TLV core in a helical fashion. Below BEP, the TLV starts developing earlier along the blade, and once it rolls up at the leading edge, it extends upstream of the rotor, and is dissected by the leading edge of the next blade. This paper presents cavitation images in a different waterjet pump (AxWJ-2 [1,2]), for which the blade loading causes broad sheet/attached cavitation with associated instabilities over large fractions of the blade surface. Prior to our experiments at Johns Hopkins University (JHU), Chesnakas et al. [2] conducted a series of tests on an anodized aluminum version of the AxWJ-2 in a water tunnel at the Naval Surface Warfare Center (NSWC), Carderock Division, to map out the pump performance curves. Using Laser Doppler Velocimetry (LDV), they measured the velocity fields upstream of the pump, between the rotor and the stator and downstream of the stator. They also performed a series of cavitation tests at NSWC, focusing on characterization of thrust breakdown. Our observations at both BEP and below-BEP conditions highlight some key cavitation phenomena, namely, sheet cavitation on the SS surface of the rotor, alternate blade cavitation, large scale instabilities, cavitation within the rotor tip gap, in the TLV, interactions between sheet and TLV cavitation, and cavitation in the stator passage. Relevant references about previous similar observations and associated modeling efforts are summarized as we describe the observations. These images have been recorded as part of a preliminary effort to resolve the dominant flow phenomena within this pump, prior to upcoming detailed PIV measurements.

TEST FACILITY, EXPERIMENTAL SETUP, AND CONDITIONS

AxWJ-2 was designed by Michael et. al. [1] using a panel method to have a slightly higher design point than the AxWJ-1, along with higher maximum efficiency. In addition, the blades were designed to have relatively constant pressure distributions on the SS, which was expected to delay thrust breakdown. They used the Reynolds-Averaged Navier-Stokes (RANS) codes CFX and Fluent to evaluate the design, and predicted a peak efficiency of 91.4% at a flow coefficient of 0.765. Tests by Chesnakas et al. [2] show fairly good agreement, with a peak efficiency of 89% at a flow coefficient of 0.76, where the flow coefficient, φ, is defined as

$$\varphi = \frac{2\pi Q}{\Omega D^3} \tag{1}$$

Our experiments are performed in an axial waterjet pump housed in a closed-loop facility shown in Figure 1. Table 1 lists the relevant geometric parameters for this pump [1,2]. AxWJ-2 has 6 rotor blades with a tip chord length of 274.3mm with a tip clearance of 0.7mm. The stator located downstream of the rotor has 8 blades with a chordlength that decreases from 121.5mm at the hub to 97.2mm at the casing. A precision-controlled AC motor installed outside the inlet pipe drives the pump via a 50.8 mm diameter shaft that passes through a settling chamber containing two honeycombs, which reduce non-uniformities and large-scale turbulence at the pump inlet. The transparent acrylic pump casing, rotor blades, and half the stator blades are optical refractive indexed-matched with the pumped fluid, a concentrated solution of sodium iodide in water (62% - 64% by weight). Matching of refractive indices is achieved by adjusting the concentration and temperature of the solution. The specific gravity of this liquid is 1.8, and its kinematic viscosity is

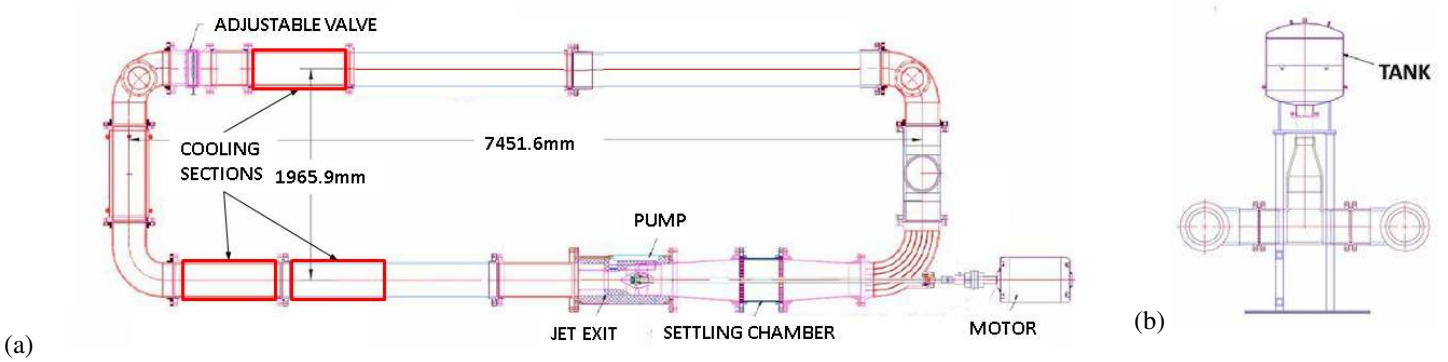

FIGURE 1 (a) TOP AND (b) SIDE VIEWS OF THE TEST FACILITY.

1.1×10^{-6} m^2s^{-1} [28]. Refractive index-matching and flat surfaces on the top and side outer walls of the casing enable us to observe and perform unobstructed high-speed image acquisition from any desired direction. Cavitation images are recorded at different cavitation indices, defined as

$$\sigma = \frac{p_{inlet} - p_v}{\frac{1}{2}\rho U_{tip}^2} \quad (2)$$

For the NaI solution, the vapor pressure ranges from 0.8 to 2kPa, with increasing temperature from 15.5 to 28.5°C. Because of its effect on cavitation index, the temperature of the fluid is monitored throughout the experiment using a thermistor installed downstream of the pump. The rotor blade tip velocity (U_{tip}) is 14.31ms^{-1}, corresponding to an angular rotation speed of 900rpm. The inlet pressure is measured using a tap located upstream of the pump. The pump is operated at BEP and below-BEP conditions, corresponding to φ=0.764 and φ=0.745. The flow rate is measured by a pitot tube installed downstream of the pump.

Number of rotor blades	6
Number of stator blades	8
Tip profile chord length c	274.3 mm
Tip profile axial chord length c_A	127.4 mm
Stagger angle $\gamma = \arcsin(c_A/c)$	27.7°
Rotor diameter D_R	303.8 mm
Casing diameter D	305.2 mm
Tip clearance h	0.7 mm
Clearance to casing diameter ratio $2hD^{-1}$	4.6×10^{-3}
Blade pitch at the tip ς	159.1 mm
Solidity at the tip $c\varsigma^{-1}$	1.72
Rotor angular velocity Ω	94.2 $rads^{-1}$ (900 rpm)
Tip velocity U_{TIP}	14.31 ms^{-1}
Blade chord Reynolds number $Re_C = U_{TIP}C\nu^{-1}$	3.6×10^6

TABLE 1: ROTOR GEOMETRY AND REFERENCE DATA

Figure 2 illustrates the pump geometry and the two locations of the high-speed camera, No. 1 and 2, relative to the pump during the observations, as viewed from outside the loop. To obtain adequate illumination of the cavitation, multiple light sources behind diffusers are placed around the pump. The resolution of the images is 2k × 2k pixels, and they are recorded at a rate of 1170 frames per second (fps), corresponding to 13 images per blade passage at 900rpm. An exposure time of 40μs is used for each image.

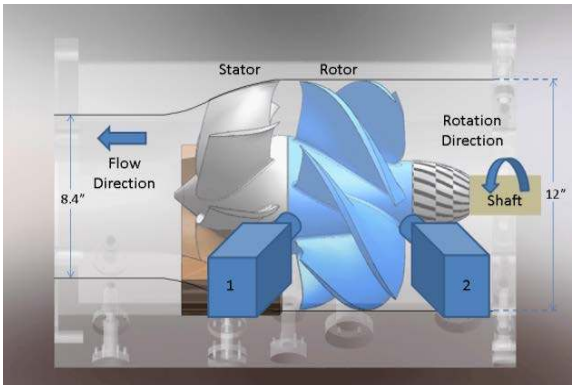

FIGURE 2: INVESTIGATED AXIAL WATERJET PUMP (AxWJ-2) AND CAMERA LOCATIONS.

RESULTS AND DISCUSSION

This section contains some preliminary observations of cavitation occurring within the pump, focusing on four main features: sheet cavitation along the SS surface of the rotor, bubbly streaks across the rotor tip gap, the signature of the rolled-up TLV, and attached cavitation along the stator leading edge. The behaviors of cavitation at and below BEP display similar trends, but there are also differences, which are highlighted in the discussions that follow.

Both at BEP and below BEP conditions, the earliest form of cavitation appears in the tip gap as long streaks of bubbles that start at the PS tip corner and extend into the blade passage. Subsequently, the bubbles are entrained into the TLV. Figure 3a shows a close-up image of the cavitation across the tip gap below BEP conditions, at σ = 0.466. As the cavitation number is lowered, sheet cavitation develops on the SS of every rotor blade. Cavitation starts at the tip corner of the leading edge, and with a slight decrease in pressure, extends towards the hub. This cavity has the appearance of a 'glassy' surface, and at BEP conditions, is thin. Below BEP conditions, the sheet cavitation thickens, as shown in Figure 3b (σ = 0.279). With decreasing

flow rate (below BEP), the incidence angle of the flow entering the passage relative to the blade increases, and with it, the blade loading. As a result, the backward leakage flow also increases, further increasing the incidence angle relative to the blade in the tip region. Consequently, the sheet cavitation on the suction surface thickens in the tip region. Accordingly, the chord-wise length of the sheet cavitation increases in the radial direction, peaking near the tip, and forming a triangular shape. The dimensions of this cavity fluctuate, and typically vary in chord-wise length and radial location by about 5%.

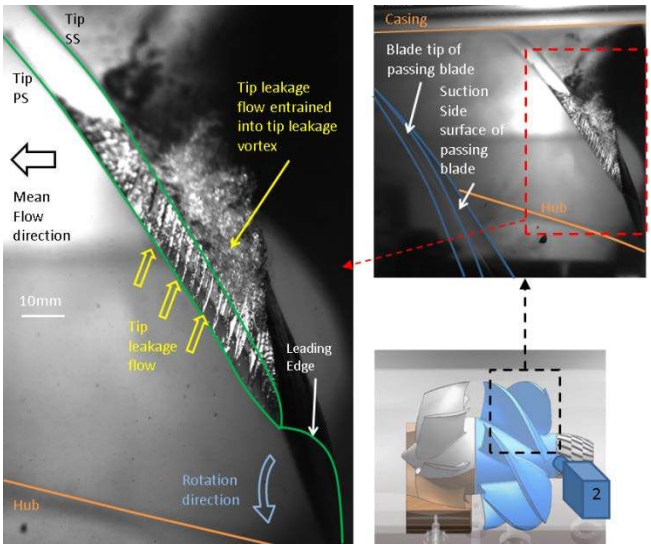

(a)

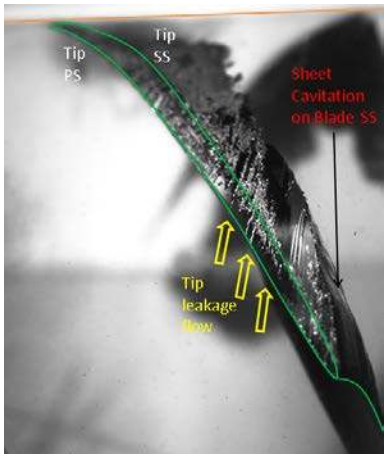

(b)

FIGURE 3: MAGNIFICATION OF (a) CAVITATION IN THE TIP GAP ENTRAINED INTO THE TLV AT BEP (σ = 0.466, ϕ =0.764), AND (b) SHEET CAVITATION ON BLADE SUCTION SIDE SURFACE BELOW BEP (σ = 0.279, ϕ =0.745). IMAGES TAKEN FROM CAMERA LOCATION 2.

The trailing edge of the sheet cavity appears to be closed in regions located away from the blade tip. The re-entrant jet that can be observed through the transparent surface, especially as it widens in the tip region (Figure 4), flows radially outward. This behavior appears to be similar to that observed on wall-bounded swept hydrofoils [30-32]. Laberteaux and Ceccio [31] observed that the laterally directed re-entrant jet eventually impinged on the cavity surface near the wall, causing formation of an open cavity with shed bubbly clouds. In the present setting, the radial re-entrant flow is entrained into the TLV, forming an unstable and noisy spiraling pattern, as shown in Figure 5. It is possible that in Laberteaux and Ceccio's [31] setting, hub vortices characterizing wing-body junctions might have also played a role.

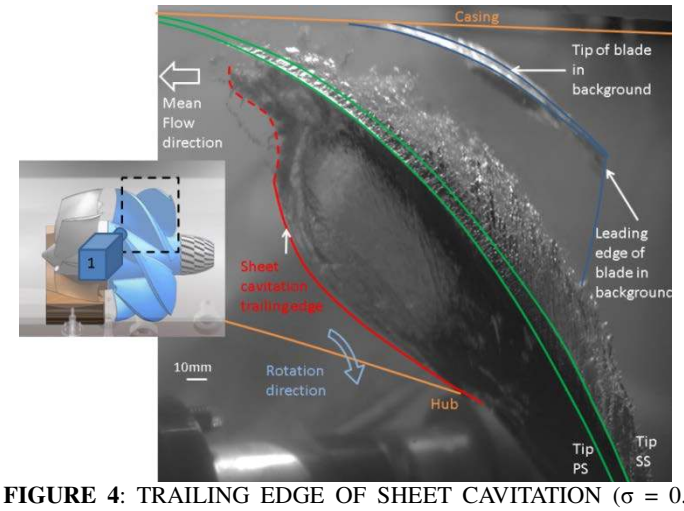

FIGURE 4: TRAILING EDGE OF SHEET CAVITATION (σ = 0. 279, ϕ = 0.745). FULL RED LINE INDICATES THE CLOSED REGION OF THE TRAILING EDGE, AND DASHED RED LINE INDICATES THE OPEN REGION. IMAGES TAKEN FROM CAMERA LOCATION 1.

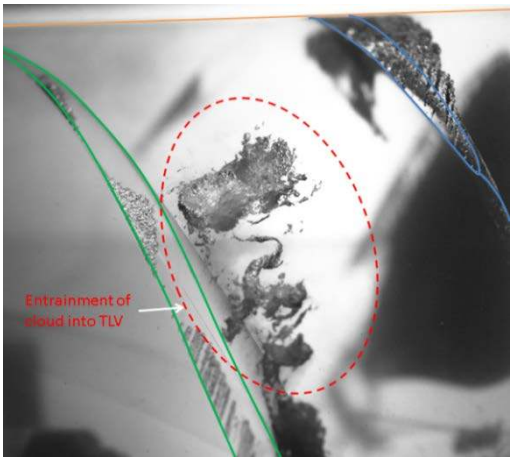

FIGURE 5: TIP LEAKAGE CAVITATION SECONDARY STRUCTURES FORMED BY ENTRAINMENT OF CLOUD OF BUBBLES INTO TLV (σ = 0. 279, ϕ =0.745). IMAGES TAKEN FROM CAMERA LOCATION 2.

Figure 6 shows a sequence of consecutive images of the cloud of bubbles as they are entrained and transported by the TLV. Once entrained, the spiraling cavitation migrates towards PS of the oncoming neighboring blade, while the large cavities rapidly disappear, leaving only a cloud of small bubbles. The TLV migration is induced by the "mirror image" of the vortex on the other side of the casing. Disappearance of the large cavities within the TLV indicates that it consists of multiple structures, and does not have a distinct central, low-pressure core. Velocity measurements and observations on cavitation in the tip region of AxWJ-1 by Wu et al. [19], whose TLV initially has a distinct core with spiraling structures around it, indicate that the distinct core disappears due to vortex breakup/bursting induced by adverse pressure gradients.

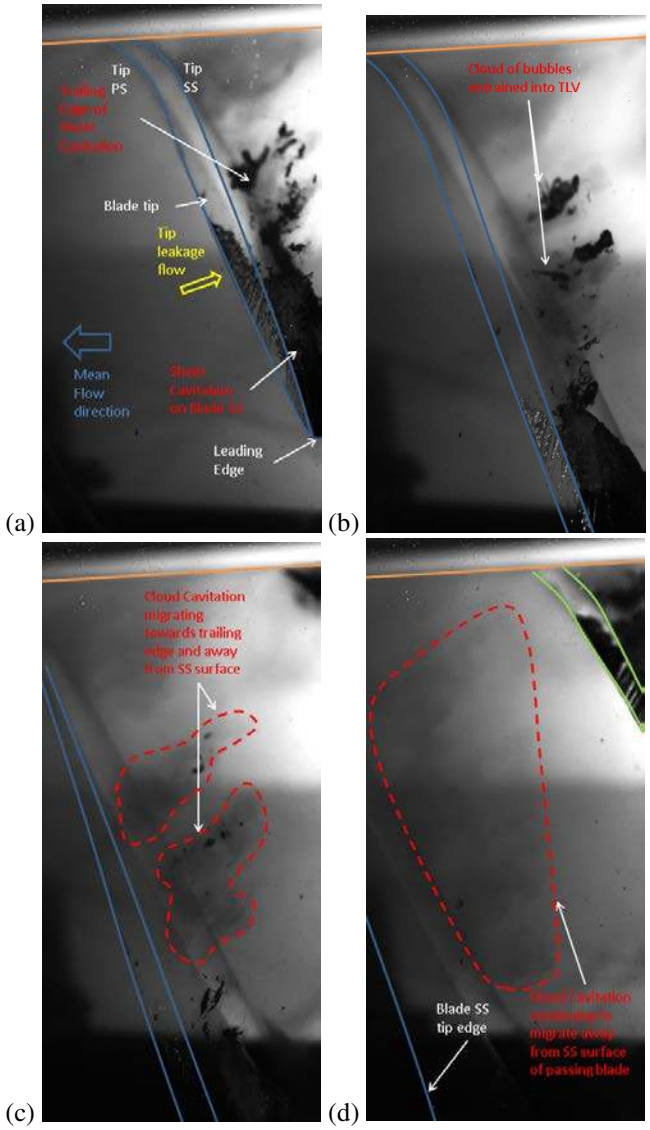

(a) (b) (c) (d)

FIGURE 6: FORMATION AND MIGRATION OF CLOUD CAVITATION FROM SHEET CAVITATION TRAILING EDGE (σ = 0.466, ϕ = 0.745), AT INTERVALS OF 2.56MS (Δt). (a) CAVITATION SHED OFF SHEET CAVITATION TRAILING EDGE (t = t0). (b) SHED CAVITIES TRANSITIONING TO CLOUD CAVITATION (t = t0+Δt). (c) CLOUD CAVITATION MIGRATING AWAY FROM SS SURFACE (t = t0+2Δt). (d) CLOUD CAVITATION APPROACHING PS SURFACE OF ONCOMING BLADE (t = t0+3Δt). IMAGES TAKEN FROM CAMERA LOCATION 2.

The location and trajectory of the TLV at BEP and σ = 0.237 is elucidated by the sequence of images presented in Figure 7. In this case, it seems that two vortices are shed from the blade tip, the first from the forward part of the blade, ~30% of the blade chord, and the second from the aft part, starting from ~70% of the chord. Both are initiated by a tip leakage flow that seems to be centered in two distinct locations. The forward TLV consists of a series of distinct spiraling structures that migrate away from the blade, but do not reach the pressure side of the neighboring blade, unlike the trend observed by in AxWJ-1. The aft vortex remains close to the blade before disappearing.

Within a certain cavitation index range (φ=0.764, $0.22 \leq \sigma \leq 0.28$), the behavior of the sheet cavity transitions from cavitation on all blades to persistent alternate blade cavitation, for which cavitation occurs in every other blade. At the high pressure side of this transition, the thickness of the sheet cavity increases noticeably, especially near the tip, and the sheet cavity on every other blade begins to expand and contract rapidly over a broad area. As an example, at φ=0.764, σ = 0.237 the radial extent of the sheet cavitation shrinks from 70% of the leading edge (Figure 7a) to less than 10%, in about 5ms (Figure 7d), but the chord-wise length of the cavity does not change significantly. Outside this transition range, these oscillations are not present. This transition range is further characterized by a loud low-frequency noise, and visible blade vibrations (more than at any other σ). Instabilities and mechanisms involved with formation of alternate blade cavitation have been seen and investigated before, predominantly in inducers of rocket turbopumps. Using potential flow based stability analysis for a two-dimensional cascade with a cavitating region, Horiguchi et al. [15] identify an amplifying mode that corresponds to this transition. They find that this statically unstable mode appears in a flow with equal length cavitation (i.e. on all blades) when the length of the cavitation exceeds 65% of the blade circumferential spacing. This mode is not present for alternate blade cavitation, hence, leading them to conclude that cavities longer than 65% of the blade circumferential spacing are statically stable during alternate blade cavitation.

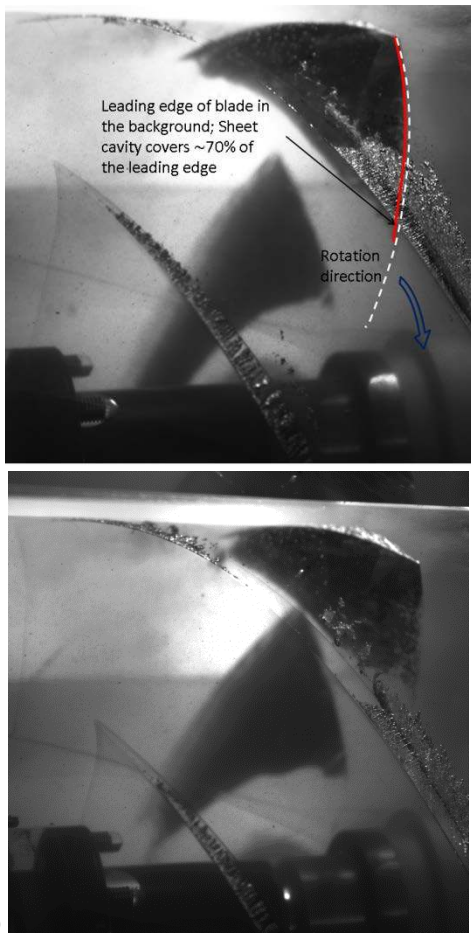

(a) (b)

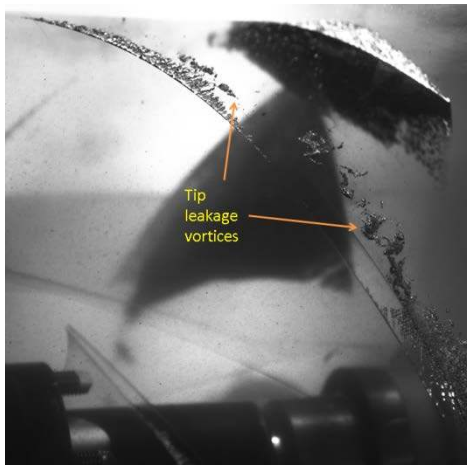

(c)

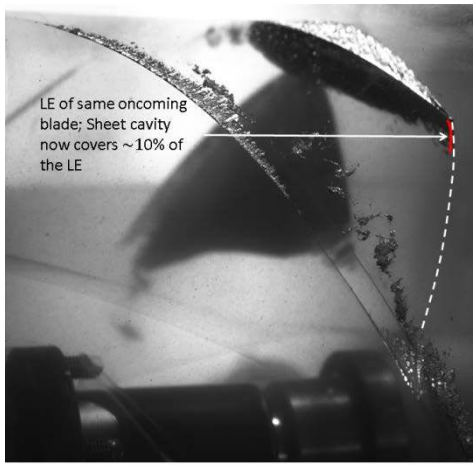

(d)

FIGURE 7: SEQUENCE OF IMAGES AT σ = 0.237, ϕ = 0.764, AT INTERVALS OF 1.71ms (Δt), SHOWING TIP GAP FLOW BEING ENTRAINED INTO THE TLV AND SAMPLE OF RAPIDLY CONTRACTING SHEET CAVITY. WHITE DASHED LINE REPRESENTS THE ROTOR BLADE LEADING EDGE. THE RED LINE INDICATES THE RADIAL EXTENT OF THE SHEET CAVITATION. (a) SHEET CAVITATION ON BLADE IN BACKGROUND IS AT ITS MAXIMUM EXTENT (t = t0). (b) BLADE IN FOREGROUND WITH CAVITATION IN TIP GAP AND SLIGHT TLV SIGNATURE (t = t0+Δt). (c) TWO TLVS DEVELOPED ON THE SS TIP CORNER OF THE BLADE IN FOREGROUND (t = t0+2Δt). (d) SHEET CAVITATION ON BLADE IN BACKGROUND AT ITS MINIMUM EXTENT (t = t0+3Δt). IMAGES TAKEN FROM CAMERA LOCATION 1.

For φ=0.764, 0.13≤σ≤0.2, stable periodic alternating cavitation persists in the rotor passage. Within this range, a relatively stable cavitating region on one blade becomes much larger than that in the neighboring one. This trend is consistent with observations performed in the context of turbopump inducers by Bordelon et al. [10], Goirand at al. [11], and Huang et al. [12], as well as computationally analyzed by Poufarry et al. [13] using RANS. Figure 8 shows a pair of images at alternate blade cavitation conditions, the first with the "heavily-cavitating" blade (outlined in blue) in the foreground of Figure 8a, and the second with the "less-cavitating" blade (outlined in green) in the foreground of Figure 8b. The sheet cavitation on the SS surface in figure 8a extends over a large fraction of the SS surface. Tip leakage flow is evident on both the "heavily-cavitating" and "less-cavitating" blades. One physical explanation of this phenomenon by Tsujimoto [16] is that as the sheet cavity grows past a certain size, the local flow near the cavity trailing edge is inclined towards the suction surface of the blade with the large cavity. As a result the incidence angle to the neighboring blade is reduced. Consequently, this blade's loading decreases, and the cavity size shrinks. In agreement with the predictions by Horiguchi et al. [15] of a critical blade cavitation length of 65%, when alternate blade cavitation starts in the present pump, the cavity length is 50 to 60% of the blade spacing, but as the cavitation index is reduced further, the cavitation on the "heavily-cavitating" blade covers a substantial part of its surface. At this phase, the triangular shape of the cavitation persists, i.e. it is longer in the tip region. The previously mentioned radially outward re-entrant flow, which is entrained into the TLV is also clearly evident.

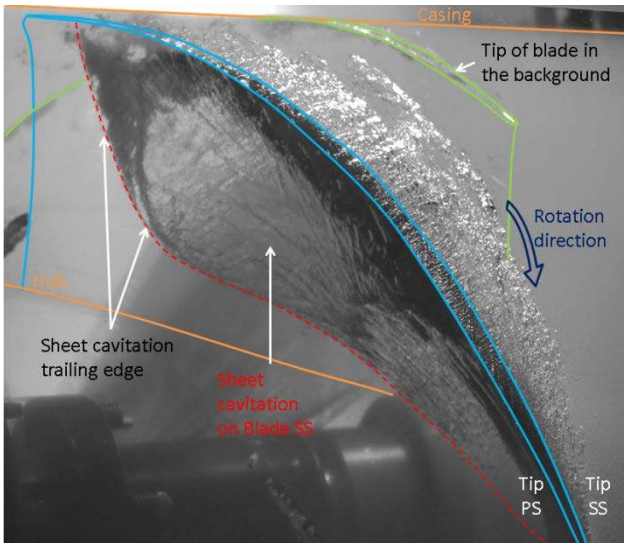

(a)

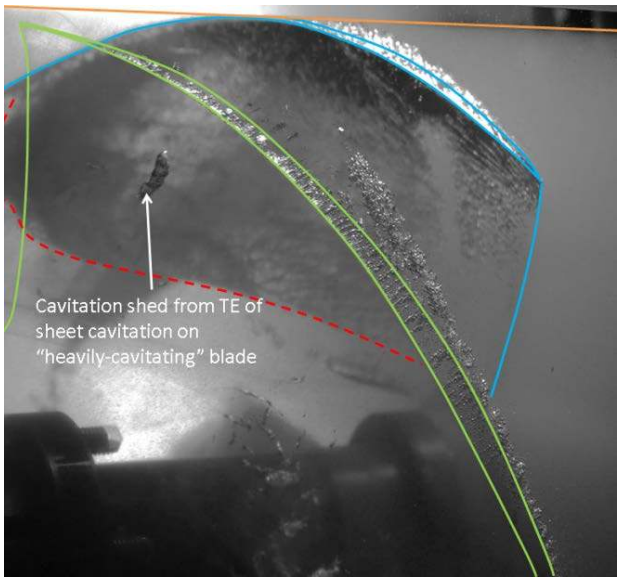

(b)

FIGURE 8: SAMPLES OF ALTERNATE BLADE CAVITATION ON SEQUENTIAL ROTOR BLADES AT σ = 0.164, ϕ =0.764. (a) A BLADE WITH MORE CAVITATION IS FOLLOWED BY (b) BLADE WITH LESS CAVITATION WITH A "HEAVILY-CAVITATING" ONE IN THE BACKGROUND. IMAGES TAKEN FROM CAMERA LOCATION 1.

In order to demonstrate the sheet cavitation more clearly, in Figure 9 we set the focus deeper into the pump, close to the SS surface of the oncoming blade. Note that we are looking through the "less-cavitating" blade located in the foreground. Figure 9 also shows the presence of hub cavitation at the blade-hub junction. Hub cavitation extends in a chord-wise direction along the root of the rotor blade. Although Figures 7-9 describe alternate blade cavitation for BEP condition, this behavior also persists below BEP. Figure 4 is an example of alternate blade cavitation below BEP, with the "heavily-cavitating" blade in the foreground.

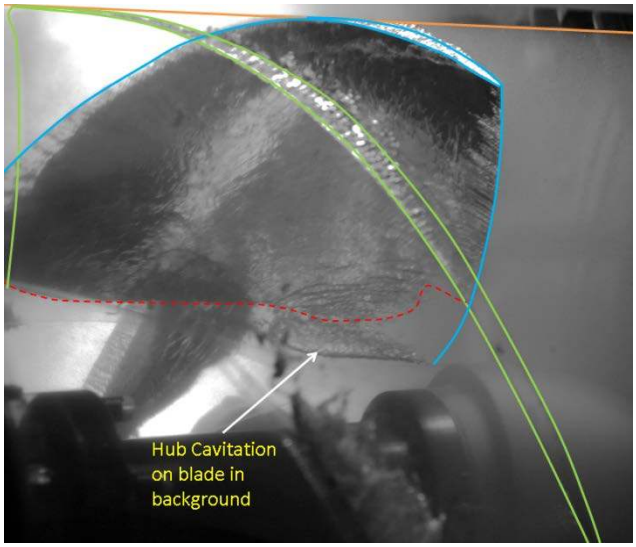

(b)

FIGURE 9: HUB AND SHEET CAVITATION ON THE CAVITATING ROTOR BLADE DURING ALTERNATE BLADE CAVITATION AT σ = 0.164, ϕ =0.764, WITH THE "LESS-CAVITATING" BLADE IN THE FOREGROUNDS. IMAGE TAKEN FROM CAMERA LOCATION 1.

As the rotor wake arrives to the stator, it induces intermittent changes to the incidence angle on the stator, and consequently, causes periodic attached cavitation along the stator leading edge. The duration of each attached cavitation event on the stator increases as the cavitation number is reduced, and it occurs at both alternate blade cavitation and non-alternate blade cavitation conditions. However, during alternate blade cavitation on the rotor blade, the stator sheet cavitation starts forming just before the trailing edge of the "heavily-cavitating" rotor blade is aligned with the leading edge of the stator blade. As the blade passes, the size of the sheet cavitation grows and extends towards hub. Bubbly "strings" form and then shed from the trailing edge of the cavitation, as shown in Figure 10a. Conversely, when the "less-cavitating" rotor blade is about to be aligned to the same stator blade, much less cavitation appears along the leading edge (Figure 10b). This cyclic behavior is likely a result of the reduced flow rate through the blade passage with the large cavitation. In their simulations of inducer blade cascades using a 2D RANS model, Fortes-Patella et al. [33] found that during alternate blade cavitation, the flow rate through the passage containing the suction surface with the large cavity is lower than that in the "less-cavitating" passage. The main cause of this phenomenon is cavity-induced blockage, which diverts part of the flow towards the neighboring channel. Because the fluid leaving the blade passage has a circumferential velocity component imparted by the rotor blades, the flow out of the cavitating passage impinges on the stator blade just before it becomes aligned with "heavily-cavitating" rotor blade. With a reduced axial flow, and assuming the same circumferential velocity, the incidence angle on the stator blade increases, enhancing the extent of sheet cavitation (Figure 10a). When the "less-cavitating" blade is about to arrive at this stator blade leading edge (Figure 10b), the axial flow increases, and the incidence angle decreases, reducing the extent of cavitation along the leading edge of the stator.

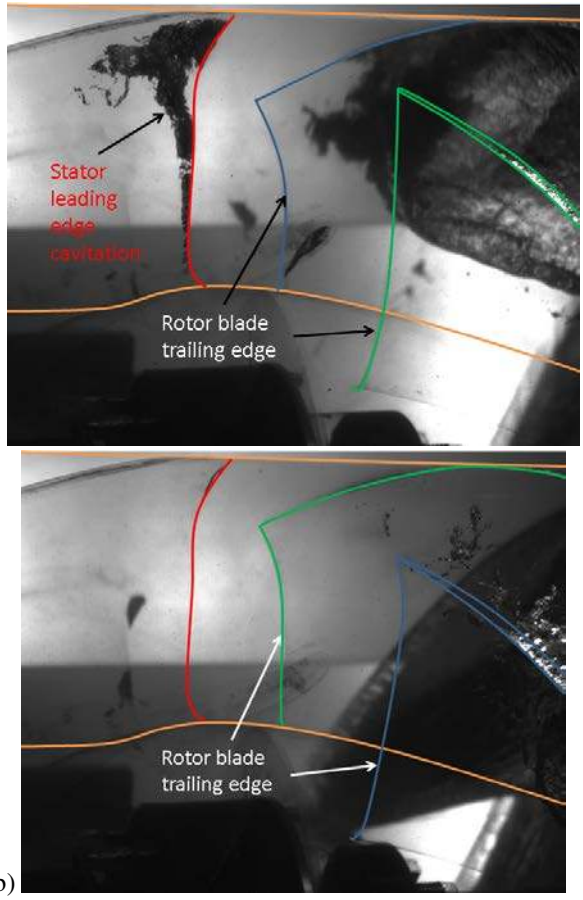

(a)

(b)

FIGURE 10: (a) CAVITATION ON THE STATOR LEADING EDGE RESULTING FROM FLOW FROM "HEAVILY-CAVITATING" BLADE (OUTLINED IN BLUE) CONVECTED TO STATOR LEADING EDGE. (b) LITTLE CAVITATION IS FORMED WHEN FLOW FROM "LESS-CAVITATING BLADE (OUTLINED IN GREEN) IS CONVECTED TO THE STATOR LEADING EDGE. IMAGES TAKEN AT σ = 0.166, ϕ = 0.764, AND FROM CAMERA LOCATION 1.

Highly unsteady sheet cavitation reappears when the cavitation number is reduced further to σ=0.13 (φ=0.764), with the cavitation expanding and contracting on the previously non-cavitating blade, covering almost 90% of the blade, and disappearing again. The initiation of this behavior appears to occur when the trailing edge of the cavity on the "heavily-cavitating" blade reaches the trailing edge of the rotor blade. Figure 11 shows a sample sequence of this phenomenon, where, within a span of about 7.7ms, the size of the cavitation

on the “less-cavitating” blade changes from having minimal cavitation near the blade leading edge to having sheet cavitation almost as extensive as the “heavily-cavitating” blade. This phenomenon is also noisy. These oscillations diminish as the cavitation number is lowered further, and reach a phase where all the blades are cavitating with sheets that cover the entire SS surface.

(a)

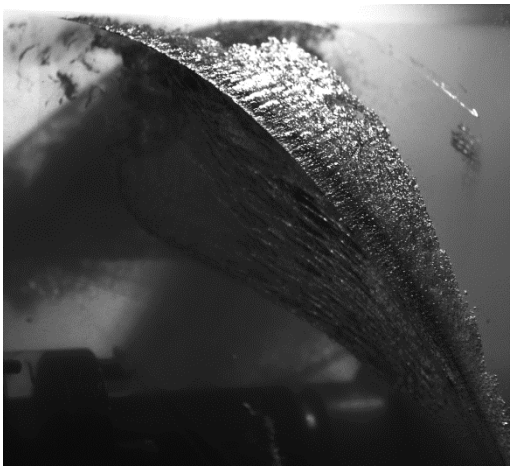

(b)

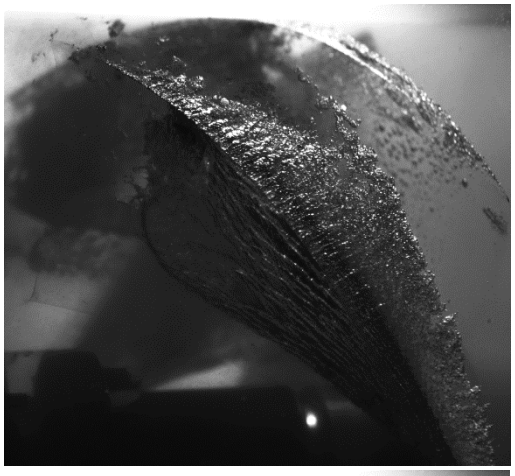

(c)

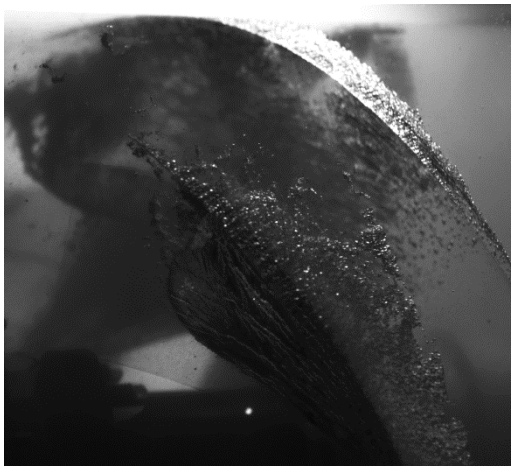

(d)

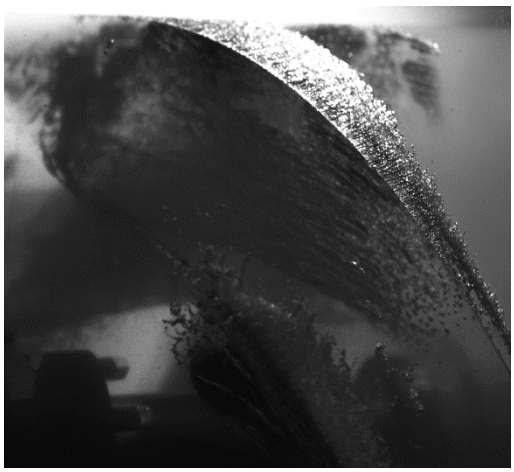

FIGURE 11: SEQUENCE OF IMAGES AT $\sigma = 0.130$, $\phi = 0.764$, AT INTERVALS OF 2.56ms (Δt), SHOWING THE START OF SHEET CAVITY OSCILLATIONS ON NON-CAVITATING BLADES. (a) LESS-CAVITATING BLADE IS IN THE BACKGROUND, WITH MINIMAL CAVITATION ON THE BLADE LEADING EDGE ($t = t0$). (b) BUBBLY CAVITATION FORMING ON LESS-CAVITATING BLADE CLOSE TO BLADE LEADING EDGE ($t = t0+\Delta t$). (C) SHEET CAVITATION BEGINNING TO FORM ($t = t0+2\Delta t$). (D) PREVIOUSLY LESS-CAVITATING BLADE NOW IN FOREGROUND, WITH CAVITATION ALMOST AS EXTENSIVE AS HEAVILY-CAVITATING BLADE ($t = t0+3\Delta t$). IMAGES TAKEN FROM CAMERA LOCATION 1.

CONCLUSION

This paper presents and discusses a series of high-speed images showing various cavitation phenomena around the rotor and stator of an axial waterjet pump (AxWJ-2) both at and below BEP. The observations are performed using a transparent pump in an optically index-matched facility, which facilitates unobstructed view of the cavitation. A number of characteristic phenomena have been observed:

First, cavitation first appears as bubbly streaks crossing the tip gap from the pressure to the suction sides of the blade. The bubbly streaks are subsequently entrained into the TLV. In the present pump, the tip leakage flow is high in two regions, the first located in the forward part, and the second centered in the aft part of the rotor blade, each leading to rollup of a TLV. The forward vortex migrates towards the neighboring blade, but does not reach it, and the aft structure remains close to the rotor SS corner. Under all of the present flow conditions, the TLV does not have a distinct core. Instead, the entrained bubbles appear as spiraling structures that persist for a while, and then disappear as a bubbly cloud.

Second, sheet cavitation appears along the SS surface of the rotor, initially near the tip, and then, with decreasing cavitation index, extends toward the hub and the blade trailing edge. At BEP, the sheet cavitation is thin, but thickens with decreasing flow rate. A radial re-entrant flow develops under the trailing edge of the sheet cavitation, which is subsequently entrained into the TLV, similar to phenomena observed on swept bounded fixed wings by Laberteaux and Ceccio [31].

Third, at a certain cavitation number, the sheet cavity begins to expand and contract rapidly in one of every two blades. With further reduction in pressure, persistent, steady alternating cavitation occurs, namely, the sheet cavitation covers much larger area and there is substantially more tip leakage cavitation on one blade compared to those on the neighboring one. The transitional instability and eventual formation of alternate blade cavitation occur when the cavity length reaches 50-60% of the blade spacing, consistent with the critical cavity length value of 65% predicted by Horiguchi et al. [15]. Based on numerical simulations of the flow field around alternate blade cavitation, Tsujimoto [16] explains that this phenomenon occurs when the sheet cavity grows past a certain size, and the local flow near the cavity trailing edge starts to interact with the leading edge of the next blade, reducing the incidence angle around the leading edge of the next blade. Consequently, this blade's loading decreases, and the cavity size shrinks. With further decrease in pressure, as the sheet cavitation covers a large fraction of the blade, the cavitation on the "less-cavitating" blade reappears, initially intermittently, and with further reduction in pressure steadily. Finally, during alternate blade cavitation, as the relatively low speed flow passing through the cavitating passage arrives to the stator, it intermittently increases the incidence angle on the stator blade, causing periodic sheet cavitation along the stator leading edge. The flow phenomena involved with the tip leakage flow, TLV structure and instabilities associated with the cavitation will subsequently be investigated using high speed PIV, with the present preliminary observations providing guidance and motivation.

ACKNOWLEDGMENTS

This project is sponsored by the Office of Naval Research under grant number N00014-09-1-0353. The program officer is Ki-Han Kim. Funding for the upgrades to test facility is provided by ONR DURIP grant No. N00014-06-1-0556. We would like to thank Yury Ronzhes and Stephen King for their contributions to the construction and maintenance of the facility, as well as to Dr. Huixuan Wu and other colleagues for their help in the preparation of the experiments. The authors acknowledge the financial support of the Spanish Ministry of Science and Innovation under the Project BES-2010-037565 that enabled the involvement and assistance of Jens Keller.

NOMENCLATURE

σ	Cavitation number
ρ	Density of the working fluid
p_{inlet}	Static pressure in the inlet flow
p_v	Vapor pressure of sodium iodide
D	Casing diameter
Ω	Rotor angular velocity
Q	Flow rate
φ	Flow coefficient
U_{tip}	Tip velocity of the rotor blade

REFERENCES

[1] Michael, T. J., Schroeder S. D., and Becnel A. J., 2008, "Design of the ONR AxWJ-2 Axial Flow Water Jet Pump," Technical Report No. NSWCCD-50-TR-2008/066, Naval Surface Warfare Center, Carderock Division, West Bethesda, MD.

[2] Chesnakas, C. J., Donnelly, M. J., Pfitsch, D. W., Becnel, A. J., and Schroeder, S. D., 2009, "Performance Evaluation of the ONR Axial Waterjet 2 (AxWJ-2)," Technical Report No. NSWCCD-50-TR-2009/089, Naval Surface Warfare Center, Carderock Division, West Bethesda, MD.

[3] Arndt, R. E. A., 1991, "Recent advances in cavitation research," Adv. Hydrosci. 12: pp. 1-78.

[4] Hammit, F. G., 1980, Cavitation and multiphase flow phenomena, McGraw-Hill, New York.

[5] Knapp, R. T., Daily, J. W., and Hammit, F. G., 1970, Cavitation, McGraw Hill, New York.

[6] Benjamin, T. B., and Ellis, A. T., 1966, "The Collapse of Cavitation Bubbles and the Pressures Thereby Produced Against Solid Boundaries," Philos. Trans. R. Soc. London Ser. A 260: pp. 221-40.

[7] Chapman, R. B., and Plesset, M. S., 1972, "Non-Linear Effects in the Collapse of a Nearly Spherical Cavity in a Liquid," Trans. ASME, J. Basic Eng. 94: pp. 142-46.

[8] Gibson, D. C., 1968, "Cavitation Adjacent to Plane Boundaries," Proc. Aust. Conf. Hydraul. and Fluid Mech., Third, pp. 210-14. Sydney: Inst. Eng.

[9] Acosta, A. J., 1958, "An Experimental Study of Cavitating Inducer," Proceedings of the Second Symposium on Naval Hydrodynamics," ON/ACR-38, pp. 537-557.

[10] Bordelon, W. J., Gaddis, S. W., and Nesman, T. E., 1995, "Cavitation Environment of the Alternate High Pressure Oxygen Turbopump Inducer," ASME FED-Vol. 210, pp. 39-46.

[11] Goirand, B., Mertz, A-L., Joussellin, F., and Rebattet, C., 1992, "Experimental Investigations of Radial Loads Induced by Partial Cavitation with Liquid Hydrogen Inducer," IMechE, C453/056, pp. 263-269.

[12] Huang, J. D., Aoki, M., and Zhang, J. T., 1998, "Alternate Blade Cavitation on Inducer," JSME International Journal, Series B, 41, No. 1, pp. 1-6.

[13] Pouffary, B., Patella, R. F., Reboud, J-L, and Lambert, P-A, 2008, "Numerical Analysis on Cavitation Instabilities in Inducer Blade Cascade," J. Fluids Eng., Vol. 130, 041302.

[14] Semenov, Y., and Tsujimoto, Y., 2003, "A Cavity Wake Model Based on the Viscous/Inviscid Interaction Approach and its Application to Nonsymmetric Cavity Flows in Inducers," J. Fluids Eng., Vol. 125, pp. 758-766.

[15] Horiguchi, H., Watanabe, S., Tsujimoto, Y., and Aoki, M., 2000, "A Theoretical Analysis of Alternate Blade Cavitation in Inducers," J. Fluids Eng., Vol. 122, pp. 156-163.

[16] Tsujimoto, Y., 2001, "Simple Rules for Cavitation Instabilities in Turbomachinery," CAV 2001: Fourth International Symposium on Cavitation, June 20-23, 2001, California Institute of Technology, Pasadena, CA USA.

[17] Miorini R. L., Wu H., and Katz J., 2011, "The Internal Structure of the Tip Leakage Vortex within the Rotor of an Axial Waterjet Pump," J. Turbomach., Vol. 134(3), 031018.

[18] Wu H., Miorini R. L., Katz J., 2011, "Measurements of the Tip Leakage Vortex Structures and Turbulence in the Meridional Plane of an Axial Water-Jet Pump," Exp. Fluids, Vol. 50, pp. 989-1003.

[19] Wu H., Miorini R. L. and Katz J., 2011, "Three-Dimensional Flow Structures and Associated Turbulence in the Tip Region of a Waterjet Pump Rotor Blade", Exp. Fluids, Vol. 51, pp. 1721-1737.

[20] Denton J.D., 1993, "Loss Mechanisms in Turbomachines,". J. Turbomach., Vol. 115, pp. 621-656.

[21] Khalid S.A., Khalsa, A.S., and Waitz, I.A., 1999, "Endwall Blockage in Axial Compressors," J. Turbomach., Vol. 121, pp. 499-509.

[22] Li Y.S., and Cumpsty N.A., 1991, "Mixing in Axial-Flow Compressors .1. Test Facilities and Measurements in a 4-Stage Compressor," J. Turbomach., Vol. 113, pp. 161-165.

[23] Li Y.S., and Cumpsty N.A., 1991, "Mixing in Axial-Flow Compressors .2. Measurements in a Single-Stage Compressor and a Duct," J. Turbomach., Vol. 113, pp. 166-174.

[24] Adamczyk J.J., Celestina M.L., and Greitzer E.M., 1993, "The Role of Tip Clearance in High-Speed Fan Stall," J. Turbomach., Vol. 115, pp. 28-39.

[25] Tan C.S., Day I., Morris S., and Wadia A., 2010, "Spike-type Compressor Stall Inception, Detection, and Control," Annu. Rev. Fluid Mech., Vol. 42, pp. 275-300.

[26] Mailach R., Lehmann I., and Vogeler K., 2001, "Rotating Instabilities in an Axial Compressor Originating from the Fluctuating Blade Tip Vortex," J. Turbomach., Vol. 123, pp. 453-460.

[27] Lakshminarayana B., 1996, Fluid Dynamics and Heat Transfer of Turbomachinery, John Wiley & Sons, NJ, USA.

[28] Uzol O., Chow Y.C., Katz J., and Meneveau C., 2002, "Unobstructed Particle Image Velocimetry Measurements within an Axial Turbo-Pump using Liquid and Blades with Matched Refractive Indices," Exp. Fluids, Vol. 33, pp. 909-919.

[29] Tan, D., Wu, H., Miorini, R., Katz, J., 2011, "Turbulent Flow Structures in the Tip Region of an Axial Waterjet Pump Rotor at Off-Design Condition," Ninth International Symposium on Particle Image Velocimetry, Kobe, Japan.

[30] Laberteaux, K.R., Ceccio, S.L., 2001, "Partial Cavity flows. Part 1. Cavities forming on models without spanwise variation," J. Fluid Mech., Vol. 431, pp. 1-41.

[31] Laberteaux, K.R., Ceccio, S.L., 2001, "Partial Cavity flows. Part 2. Cavities forming on test objects with spanwise variation," J. Fluid Mech., Vol. 431, pp. 43-63.

[32] Franc, J.P., 2001, "Partial Cavity Instabilities and Re-Entrant Jet," CAV 2001: Fourth International Symposium on Cavitation, June 20-23, 2001, California Institute of Technology, Pasadena, CA USA.

[33] Fortes-Patella, R., Coutier-Delgosha, O., Perrin, J., and Reboud, J. L., 2007, "Numerical Model to Predict Unsteady Cavitating Flow Behavior in Inducer Blade Cascades," J. Fluids Eng., Vol. 129, pp. 128-135.